YIH_n: A New Family of Metal-rich Hydride Halides

Mikhail Ryazanov, Arndt Simon*, and Hansjürgen Mattausch

Stuttgart, Max-Planck Institut für Festkörperforschung

Received April 5th, 2004.

Dedicated to Professor Joachim Sieler on the Occasion of his 65th Birthday

Abstract. The graphite-like yttrium hydride halides, YIH_n ($0.8 \leq n \leq 1.0$), have been prepared in quantitative yields by heating either YI_3, YH_2 (1:2) or stoichiometric YI_3, YH_2, Y mixtures in sealed Ta ampoules at 900°C. A lower limit of the homogeneity range, $n \approx 2/3$, has been determined from dehydrogenation experiments. All YIH_n phases adopt the ZrBr-type heavy-atom structure. The hydrogen variation is accompanied by a change in the *c* lattice constant from 31.162(3) to 31.033(1) Å for $n = 0.61(3)$ to 1.02(3). The YIH_n phases reversibly react with hydrogen at 400-600°C to form the light green transparent compound YIH_2. However, increasing the reaction temperature above 700°C causes decomposition to an unidentified phase being in equilibrium with YH_2 and YI_3. The arrangement of the heavy atoms in YIH_2 ($P\bar{3}m1$; $a = 3.8579(3)$ Å, $c = 10.997(1)$ Å) corresponds to a four-layer I-Y-Y-I slab with the stacking sequence (AbaB) as was found by x-ray powder diffraction data refinement with the Rietveld method. A miscibility gap exists between YIH and YIH_2.
Samples YIH_n ($n \leq 1.0$) show metallic conductivity at room temperature, which changes into semiconducting behavior with decreasing temperature as *n* approaches its lower value $\approx 2/3$.

Keywords: Yttrium hydride halides; Metal-rich compounds; Phase relation; X-ray powder diffraction; Rietveld refinement; Resistivity measurements; Electron localization

YIH_n: Eine neue Familie metallreicher Hydridhalogenide

Inhaltsübersicht. Hydridiodide YIH_n ($0.8 \leq n \leq 1.0$) wurden in quantitativer Ausbeute als graphitfarbene Substanzen durch Erhitzen von YI_3, YH_2 (1:2) bzw. stöchiometrischen Gemengen von YI_3, YH_2, Y bei 900°C in zugeschweißten Tantalampullen präpariert. Bei Dehydrierungsversuchen wurde der minimale H-Gehalt von YIH_n mit $n = 0.61(3)$ bestimmt. Alle YIH_n Verbindungen kristallisieren im ZrBr-Typ. Mit steigendem H-Gehalt nimmt die Länge der *c*-Gitterkonstante von 31.162(3) zu 31.033(1) Å ab. Die Verbindungen YIH_n können reversibel unter Bildung der hellgrünen durchsichtigen Verbindung YIH_2 bei 400-600°C hydriert werden. Temperaturen über 700°C führen zur Zersetzung von YIH_2 unter Bildung von YH_2, gasförmigem YI_3 und einer schwarzen unbekannten Substanz. Die Schweratomstruktur von YIH_2 wurde durch Rietveld-Verfeinerung aus Röntgendaten bestimmt. Es kristallisiert in $P\bar{3}m1$, $a = 3.8579(3)$ Å, $c = 10.997(1)$ Å. Die Schweratome sind in Schichten I-Y-Y-I mit der Stapelung AbaB angeordnet. Zwischen $YIH_{1.0}$ und $YIH_{2.0}$ besteht eine Mischungslücke. YIH_n Proben mit $n \leq 1.0$ zeigen metallische Leitfähigkeit mit einem Metall-Halbleiter Übergang bei sinkenden Temperaturen und niedrigem H-Gehalt.

Introduction

The hydride halides RXH_n of scandium [1], yttrium [2] and the trivalent lanthanides [3-10] with $n \leq 1$ constitute a closely related family of metal-rich compounds. They all are graphite-like with a characteristic metallic luster and have a range of homogeneity with an upper limit $n = 1.0$. For most of the compounds [2-8] the lower limit has been found to approach a value of $n = 0.67$. These conditions imply the existence of valence electrons available for metal-metal bonding as one can infer from the ionic description $R^{3+}X^{-}(H^{-})_n(e^{-})_{2-n}$. Up to now the following phases have been synthesized and studied: $RClH_n$ (R = Sc, Y, La, Ce, Pr, Gd, Tb), $RBrH_n$ (R = Y, La-Nd, Gd, Tb) and $GdIH_n$.

Prof. Dr. Dr. h. c. mult. Arndt Simon,
Max-Planck-Institut für Festkörperforschung,
Heisenbergstr. 1,
D-70569 Stuttgart,
Fax: 0711/689/1091
E-mail: A.Simon@fkf.mpg.de

The structure of RXH_n consists of close-packed metal atom bilayers, which are sandwiched between layers of halide ions to give the stacking sequences X-R-R-X as in ZrCl [11, 12], ZrBr [13] or related "2s"-type structures [4]. The known types of packing these four-layer slabs are represented in Figure 1. The hydrogen atoms occupy tetrahedral voids between the metal atom layers [3], and filling of all the tetrahedral voids corresponds to the upper limit $RXH_{1.0}$.

Further insertion of hydrogen into the structure can be accomplished by heating RXH_n in a hydrogen atmosphere at 400-500°C. This leads to the formation of transparent and insulating RXH_2 phases, in which the additional hydrogen atoms are distributed in the trigonal voids of the metal atom layers, one atom in each basis of an antiprism [5]. There exists a gap of miscibility between RXH and RXH_2 [2, 7]. All known $RClH_2$ (R = Y, Ce, Pr, Gd, Tb, Lu), $RBrH_2$ (R = Ce, Pr, Nd, Gd, Tb) and $GdID_2$ phases [2, 8] are isotypic and exhibit the same stacking sequence (3R form) of the heavy atoms as in the high-T modification of

 DOI: 10.1002/zaac.200400094

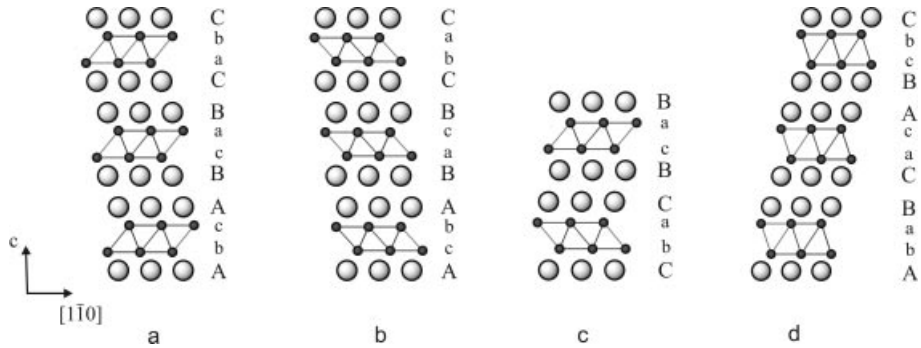

Fig. 1 Projections along [110] of the different stacking variants for the heavy-atom arrangements in hydride halides RXH_n: (a) ZrCl type, (b) ZrBr type, (c) "2s" type and (d) RXH_2 type. The small and capital letters refer to relative positions of close-packed metal and halide ion layers, respectively.

Ta_2S_2C [14]. The transition from RXH_n, to RXH_2 is accompanied by significant changes in structure. The arrangement of the halogen atoms within one XRRX slab redistributes from trigonal prismatic to trigonal antiprismatic to form a new layer sequence AbaB. Additionally, the interlayer metal-metal distances increase from 3.58 to 3.96 Å upon conversion from $TbClD_{0.8}$ to $TbBrD_2$ [5]. The changes in the atomic distances and the nonconducting behavior of RXH_2 are consistent with an ionic description as $R^{3+}X^{-}(H^{-})_2$.

While a great number of hydride monochlorides and monobromides of the rare-earth elements are known, there is much less information about the related monoiodide phases. The present paper reports on some metal-rich and salt-like compounds in the system Y/I/H, their phase relations, structural features and transport properties.

Experimental Section

Materials

Yttrium metal pieces (99.99 %; Johnson Matthey, Karlsruhe) and iodine powder (99.8 %; Merck) were used as starting materials. Yttrium triiodide was prepared by a direct reaction of the elements in a sealed quartz glass tube at 900 °C [15] and further purified by two subsequent sublimations at 830 °C in high vacuum (10^{-4} torr). YH_2 was obtained from metal pieces by hydrogenation under 1 atm H_2 (99.999 %; Messer-Griesheim) in a molybdenum boat at 400 °C following the known procedure [16]. When no more pressure change was observed the temperature was lowered to 350 °C, and the sample was pumped until the pressure was reduced to about 2 ± 10^{-3} torr, which corresponds to the equilibrium H-pressure for YH_2 at the given temperature.

Syntheses

Yttrium hydride halides, YIH_n ($n \leq 1$), were synthesized under similar conditions either from Y(filings)/YH_2/YI_3 or from YH_2/YI_3 mixtures in arc-welded tantalum tubes filled with argon. These were then sealed under vacuum in fused silica jackets and heated to the reaction temperature. All manipulations were performed with Schlenk technique or in a glove box under argon. Further preparation details are summarized in Table 1.

Hydrogenation of YIH was carried out in a Sieverts-type apparatus [17, 18] supplied with a manometer Membranovac DM12/DI2000 (Leybold), which allows to detect the pressure change during a reaction. Typically, a weighted sample of approx. 0.3-0.5 g was heated in a molybdenum boat under 1 bar H_2 in a closed calibrated volume of 370 cm^3.

Experiments on dehydrogenation were performed by heating samples covered with tantalum jackets in a quartz glass tube under dynamic vacuum (10^{-5} torr).

Characterization

a) Chemical analysis

The hydrogen content n in YIH_n was determined analytically. Weighted samples (25-50 mg) were mixed with V_2O_5 used as an oxidant and burned in an oxygen flow at 950 °C. The evolved gas passed CuO (850 °C), Ag_3VO_4 (850 °C), $Ag_2O\pm MnO_2$ (500 °C) [19], Ag-wool (500 °C), and the generated water was titrated with a Karl-Fischer coulometric detector KF 653 (Metrohm) [20]. The hydrogen content was calculated as a mean value from two independent measurements. The maximal spread of n calculated for the composition YIH_n was found to be $\Delta n = 0.03$.

b) X-ray powder diffraction

Due to their moisture- and air-sensitivity polycrystalline samples YIH_n (mixed with Si, $a = 5.4303$ Å, as an internal standard) were sealed in glass capillaries filled with Ar. X-ray diffraction patterns were recorded in Debye-Scherrer geometry on a Stoe Stadi P diffractometer (MoK_α radiation, $\lambda = 0.7093$ Å, germanium monochromator). For a number of samples the heavy-atom arrangement was refined by Rietveld analysis using the FullProf program [21]. Some details of data collection and the results of refinement are shown in Table 2. The pseudo-Voigt function was used for simulation of the peak shapes. All reflections were corrected for asymmetry ($2\theta < 40°$) and preferred orientation effects using the March-Dollase function. Guinier diagrams were recorded on a modified Guinier camera ($CuK\alpha_1$ radiation, SiO_2 monochromator) [22] with an open aperture.

c) Resistivity measurements

Electrical resistivity was measured on pressed samples in the temperature range of 8-250 K by the van der Pauw method using the

Table 1 Reaction conditions and structural data for YIH_n

N	Starting materials	Reaction condition	Product	a/Å	c/Å	V/Å^3	Type
1	YI_3/YH_2 (1:2)	4d, 900 °C	$YIH_{1.02}$	3.9349(3)	31.033(1)	416.23(6)	ZrBr
2	YI_3/YH_2 (1:2)	6d, 900 °C	$YIH_{0.98}$	3.9337(7)	31.047(6)	416.1(1)	ZrBr
3	$Y/YI_3/YH_2$ (19:20:21)	6d, 900 °C	$YIH_{0.81}$	3.9334(2)	31.096(2)	416.58(3)	ZrBr
4	$YIH_{0.98}$	20 h, 730 °C, 10^{-5} torr	$YIH_{0.79}$	3.9340(7)	31.102(6)	416.85(9)	ZrBr
5	$YIH_{0.81}$	10 h, 730 °C, 10^{-5} torr	$YIH_{0.61}$	3.9326(3)	31.162(3)	417.36(5)	ZrBr
6	$YIH_{0.81}$	10 h, 800 °C, 10^{-5} torr	$YIH_{0.59}$	3.9324(2)	31.158(2)	417.27(3)	ZrBr
7	$YIH_{0.61}$	10 h, 900 °C, 10^{-5} torr	YI_3, Y				

Table 2 Some details of data collection and structure refinement for YIH_n

	$YIH_{0.61}$	$YIH_{1.02}$	$YIH_{2.0}$
Radiation	Mo Kα	Mo Kα	Mo Kα
Detector	PSD	PSD	PSD
Profile range (°2θ)	2-65	2-65	2-65
Step size (°2θ)	0.01	0.01	0.01
Step scan time (s)	100	100	200
Number of collected points (N)	6300	5430	6300
Number of reflections	236	167	246
Number of refined parameters (P)	15	18	20
R_p	0.0257	0.0421	0.0201
R_{wp}	0.0346	0.0535	0.0321
R_{exp}	0.0246	0.0513	0.0162
R_B	0.132	0.132	0.104
S	1.41	1.04	1.97

Note: $R_p = \sum_{i=1,N} |y_i - y_{c,i}| / \sum_{i=1,N} y_i$, $R_{wp} = \left[\sum_{i=1,N} w_i |y_i - y_{c,i}|^2 / \sum_{i=1,N} w y_i^2 \right]^{1/2}$, $R_{exp} = \left[(N-P) / \sum_{i=1,N} w y_i^2 \right]^{1/2}$, $R_B = \sum_i |I_{obs,i} - I_{calc,i}| / \sum_i |I_{obs,i}|$, $S = R_{wp}/R_{exp}$.

cryostat of a PPMS magnetometer (Quantum Design). The samples were pressed together with 4 platinum contacts.

Results and Discussion

Attempts to synthesize YI_2H_n from YI_3/YH_2 (2:1) reaction mixtures by analogy with known hydride halides RI_2H_n (R = La−Nd, Gd) [18, 23-24] were unsuccessful. Heating the reagents at 820 °C revealed no reaction, while increasing the temperature to 900 °C led to the formation of YIH_n ($n \leq 1$).

Heating YI_3/YH_2 (1:2) as well as stoichiometric $YI_3/YH_2/Y$ reaction mixtures in welded tantalum tubes results in the formation of dark grey laminar YIH_n ($0.8 \leq n \leq 1.0$) phases with a metallic luster. Both synthetic approaches quantitatively yield YIH_n single phase products as has been found with other RXH_n systems (R = Sc, Y, La−Nd, Gd, Tb, Er, Lu; X = Cl, Br) [1$\bar{1}$0]. The hydrogen concentration in halide hydrides can be varied either by using the appropriate amounts of starting reagents or by heating the YI_3/YH_2 (1:2) mixture at different reaction conditions (temperature, time, permeability of the container material to hydrogen). When a metal powder is included into the reaction its possible hydrogen contamination should be considered, particularly if it was obtained by dehydrogenation of the metal hydride.

In order to determine the lower limit of the homogeneity range a series of dehydrogenation experiments for YIH_n in a dynamic vacuum was carried out. Some experimental details and product descriptions are given in Table 1. Samples 4-7 have been heated in an "open" system−tantalum tube sealed at one side and clinched at the other−for several hours until the pressure of approx. 10^{-3} torr in the system reduced to its starting value of about 10^{-5} torr. The heating of $YIH_{0.81}$ in the range of 730-800 °C leads to a reduction of the H-content to $n = 0.61(3)$. Further increase of the temperature results in decomposition of the sample into volatile YI_3 and Y, which suggests that the value $n \approx 0.67$ represents the lowest hydrogen concentration in YIH_n, similar to that in analogous YXH_n (X = Cl, Br; $0.7 \leq n \leq 1.0$) hydride halides [2].

In all the homogeneity range, $0.6 \leq n \leq 1.0$, YIH_n crystallizes with the ZrBr-type structure. The lattice constants as a function of *n* are plotted in Figure 2. There is a distinct decrease (0.13 Å) in the length of the *c* axis, whereas the *a* lattice constant slightly (0.003 Å) increases with larger *n*. Similar variations of the lattice constants were found in $RClH_n$ (R = Sc [1], Y [2]) though these are accompanied by a structural change from the ZrBr- to the ZrCl-type structure with increasing H-content. This structural rearrangement might be accounted for by a subtle charge redistribution in the metal-metal bonding. The change of the lattice constants can be rationalized in terms of an electrostatic model [18], assuming the formation of H^- anions by localization of electrons from itinerant M-M bonding. Incorporating the hydrogen ions in between double metal atom layers results in a decrease of the *c* lattice parameter due to Coulomb attraction between the M^{3+} and H^- ions, while the *a* lattice constant increases due to repulsion between the H^- ions in the layer.

The atomic distances for the phase boundaries, $YIH_{0.61(3)}$ and $YIH_{1.02(3)}$, are shown in Table 3. The differentiation of distances in the Y-Y sheets, 3.5 and 3.9 Å, indicates strong metal-metal bonding between adjacent metal atom layers and a somewhat weaker bonding between atoms in a layer. The latter is mainly dictated by the I-I distance in the close-packed anion sheets. The Y-I distances are 3.08 Å, a slightly shorter value than expected for pure ionic bonding (3.10 Å) due to the asymmetric bonding situation. The interlayer I-I contacts (4.19 Å) are 0.16 Å less than those in crystalline iodine which indicates a weak bonding between the halide

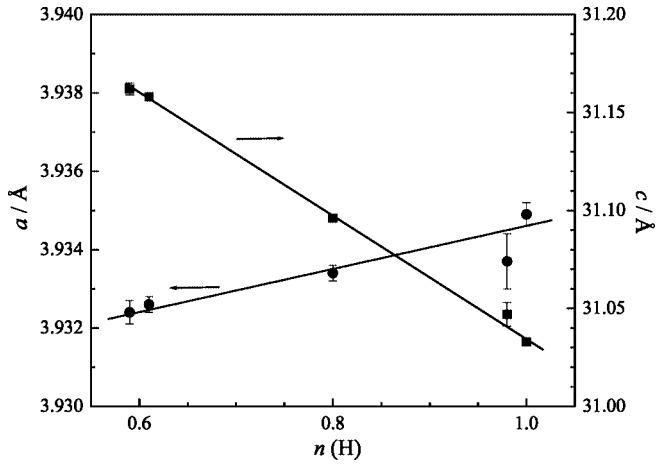

Fig. 2 Lattice constants of YIH_n as a function of *n*.

Table 3 Selected bond distances/Å in YIH_n

Compound	Y − Y	Y − I	I − I [a]
$YIH_{0.61}$	3.933(1) 3.553(8) [a]	3.071(6)	4.188(7)
$YIH_{1.02}$	3.935(1) 3.499(5) [a]	3.082(4)	4.186(4)
$YIH_{2.0}$	3.858(1) 3.851(6) [a]	3.095(4)	4.198(6)

[a] interlayer distances.

layers belonging to the neighboring IYYI slabs. Full occupation of tetrahedral voids with hydrogen yields a 0.05 Å decrease in the interlayer metal-metal distances and almost no change in other bond lengths.

It is interesting to note that the hydride chlorides of rare earth metals, $RClH_n$ (R = La, Ce, Pr, Gd) adopt the ZrBr-type stacking, while the analogous hydride bromides exhibit the ZrCl-type stacking. The two types of stacking may arise from a competition between electrostatic second nearest neighbor effects *versus* polarization effects between adjacent metal and halide ion layers. In the ZrBr-type stacking each halogen atom is arranged above a second nearest metal atom in the neighboring layer so that it allows additional attraction between the metal ions and second nearest halogen neighbors. Such a layer arrangement also favors polarization of the halide atoms by the second nearest metal atoms along the [001] direction through interstices in the neighboring halide layer (Fig. 1). The interlayer antiprismatic coordination of the halogen atoms by Cl and Zr atoms in ZrCl induces a linear arrangement of alternating pairs of metal and halogen atoms [25] in the (1-10) and equivalent (120) and (210) planes, which implies a predominant polarization of the halogen atoms by adjacent metal atoms along the X−R−R−X atomic strings. Similar effects in related CdI_2 and $CdCl_2$ structures have been pointed out by *Krebs* [26].

It appears that more "ionic" hydride chlorides crystallize rather in the ZrBr structure type, whereas for more "polarized" bromides and iodides there is no obvious benefit between the ZrBr- and ZrCl- type stacking as polarization effects, although in a different form, occur in both cases. For instance, $GdIH_{0.8}$ has been found to crystallize with both the ZrCl- and ZrBr- as well as intermediate "2s"-type structures [4]. Calculations of the Madelung part of lattice energy for $TbClD_{0.8}$ with the ZrBr- and ZrCl-type stacking sequences using the MAPLE program [27] yields an insignificantly smaller (0.02 %) energy for the latter structure.

Phase relation between YIH_n and YIH_2

Continuous heating of the YIH samples under 1 bar hydrogen in a closed system leads to light-green and transparent YIH_2. The product composition is derived from the difference of hydrogen pressure after cooling the sample. Some reaction temperatures and heating rates used for hydrogenation are listed in Table 4. Figure 3 shows the temperature dependence of the H-pressure in a system with and without the sample. A characteristic drop in pressure observed at 330 °C indicates the beginning of hydrogen absorption, which is completed at 450 °C. The lowering of the absorption temperatures with reduced heating rates is in accordance with expectations. YIH_2 can easily be dehydrogenated to the initial YIH_n phases by heating under dynamic vacuum. The absorption and desorption of hydrogen occur in the same temperature range as shown in Figure 3. Thus, the hydrogenation of YIH_n to YIH_2 is a fully reversible topochemical reaction. However, heating YIH_2 (YIH) in a hydrogen atmosphere to above 700 °C leads to decomposition of the sample with the formation of an unidentified black compound (Z) being in equilibrium with YH_2 and volatile YI_3. This process is also accompanied by liberation of hydrogen as one can conclude from a distinctive pressure increase in the system above 700 °C (Fig. 4). The pressure difference after the sample has been cooled leads to the formal composition "$YIH_{1.33}$". The I/Y ratio of the decomposition product determined by an EDX analysis on several laminar crystallites varies in the range 0.95-1.25, which overlaps in composition with that of several metal-rich cluster compounds [28]. The XRD pattern clearly differs from patterns of YIH_n ($0.6 \leq n \leq 1.0$) and YIH_2. It exhibits two sets of diffraction peaks, characteristic broad reflections and sharp ones[1)].

Crystal structure of YIH_2

The structural study of YIH_2 has been performed on polycrystalline samples since suitable singe crystals were not available. All reflections have been indexed in a primitive trigonal unit cell with $a = 3.8579(3)$ Å and $c = 10.997(1)$

[1)] d values (Å) of sharp reflections: 7.676, 3.842, 3.441, 2.562, 1.9924, 1.9224, 1.7702, 1.7230, 1.3834.

Table 4 Reaction conditions on (de)hydrogenation of YIH_n

N	Reagent	Heating condition	Product	Space group	a/Å	c/Å	V/Å3	Type
1	YIH	500 °C, 2 °/min, 1bar H_2	$YIH_{2.0}$	$P\bar{3}m1$	3.8579(3)	10.997(1)	141.74(4)	1T
2	YIH	550 °C, 2 °/min, 1bar H_2	$YIH_{2.0}$	$P\bar{3}m1$	3.8560(6)	11.001(6)	141.64(7)	1T
3	YIH	750 °C, 3 °/min, 1bar H_2	YI_3, YH_2 + Z					
4	YIH_2	750 °C, 2 °/min, 1bar H_2	YI_3, YH_2 + Z					
5	YIH_2	700 °C, 1 °/min, 10^{-5} torr[a)]	YIH_n	$R\bar{3}m$	3.9328(6)	31.094(5)	416.50(6)	ZrBr

[a)] dynamic vacuum.

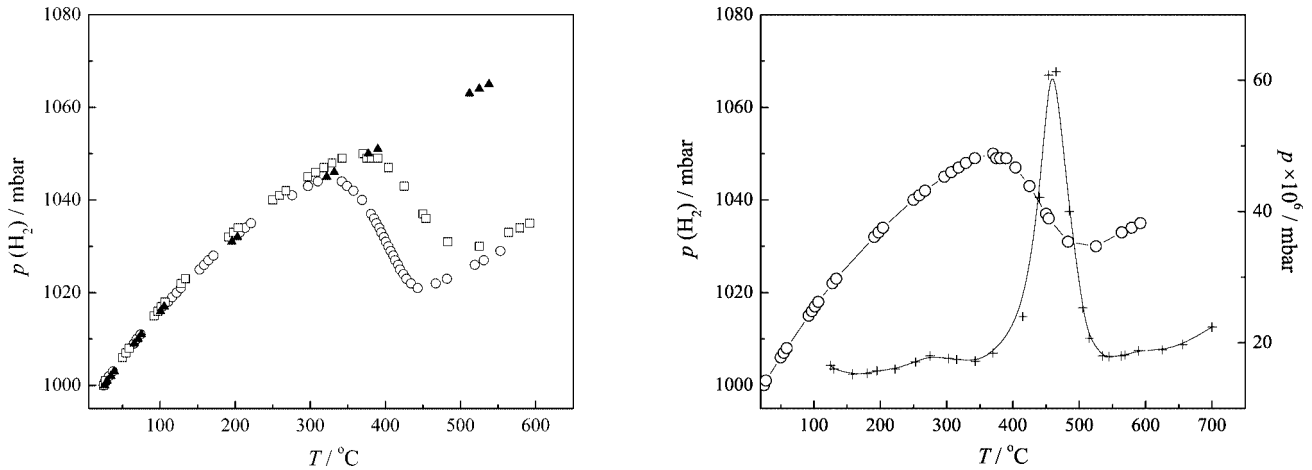

Fig. 3 Left: Temperature dependence of the hydrogen pressure upon hydrogenation of YIH at a heating rate of 3 °C/min (□) and 2 °C/min (○), respectively. Points (▲) correspond to the pressure change in an "empty" system (heating rate: 3 °C/min). Right: Temperature dependence of pressure (+) in a system upon dehydrogenation of YIH_2 under dynamic vacuum (heating rate: 1 °C/min) compared with (○) hydrogenation of YIH (heating rate: 2 °C/min).

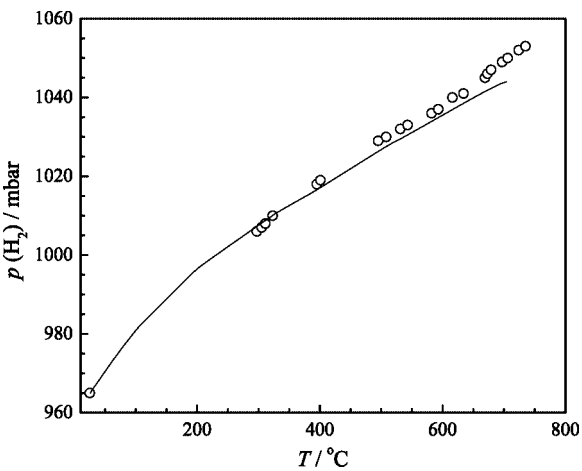

Fig. 4 Temperature dependence of the hydrogen pressure in a system with (○) and without (—) YIH_2 at a heating rate of 2 °C/min.

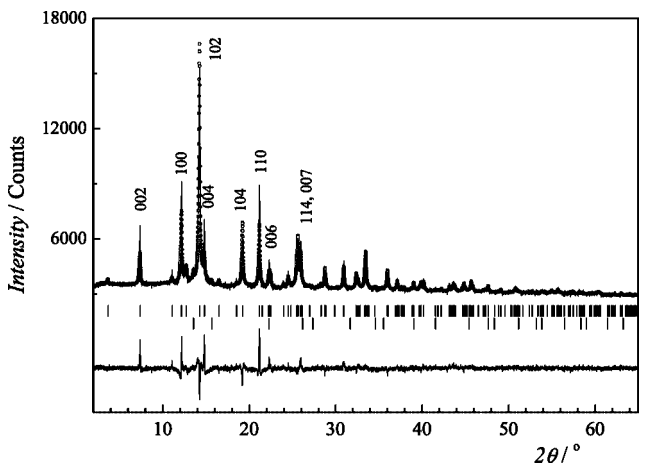

Fig. 5 (a) The final Rietveld refinement pattern of YIH_2. The calculated profile is denoted by "○"; the solid line corresponds to the observed pattern; vertical bars indicate the calculated reflection positions for YIH_2 (upper) and YH_2 (bottom). The bottom trace represents the difference between the experimental and calculated values.

Å. The arrangement of the heavy atoms has been refined from X-ray powder diffraction data by the conventional Rietveld method [29]. The analysis of the pattern profile reveals a small contamination (2 %) of the sample with YH_2. The results of the final refinement are plotted in Fig. 5. Atomic positions and selected bond distances for YIH_2 are given in Table 5 and 3, respectively. The final profile

Table 5 Atomic positions of the heavy-atom arrangement of YIH_2 [a)]

Atom	Site	x	y	z	Biso (Å^2)
Y	2d	2/3	1/3	0.3572(4)	0.8(1)
I	2d	1/3	2/3	0.1618(3)	1.8(1)

[a)] a = 3.8579(3) Å, c = 10.997(1) Å; space group: $P\bar{3}m1$

factors, R_p and R_{wp}, converged to 2.01 and 3.21 % close to an expected value R_{exp} = 1.62 %. However, there is a misfit in intensity for a number of diffraction peaks. The calculated intensities for the reflections 00*l*, *hhl* and 100 are lower than the observed ones, while those with indices 10*l* (*l* = 2n) are larger. These deviations can be attributed to preferred orientation and/or stacking defects in the "weak" direction. Both the effects occur frequently in layered compounds.

Obviously, the preferred orientation effects dominate, as the pattern taken with less penetrating $CuK\alpha_1$ radiation shows even increased deviations of the above mentioned intensities. Indeed, the Guinier diagram of a sample recorded on a modified Guinier camera [22] with an open aperture reveals a nonconstant intensity distribution along the Debye rings, which is a typical feature for samples affected by preferred orientation.

The structure of YIH_2 has the same heavy atom arrangement as in related $TbBrD_2$ [5]. It consists of close-packed bilayers of metal atoms enclosed within two close-packed halide sheets. However, in contrast to all known RXH_2 phases, the translation period of YIH_2 corresponds to one slab IYYI with the stacking sequence AbaB (1T form), which is the characteristic sequence for ZrXH (X = Cl, Br) [30] and the lanthanide carbide halides [9, 31-32]. Additional insertion of hydrogen into the structure induces a significant change in the metal-metal distances. Whereas the intra- and interlayer Y-Y distances in YIH are significantly different, 3.9 and 3.5 Å, as mentioned before this difference vanishes for YIH_2 (3.86 and 3.85 Å) due to loss of the metal-metal bonding. Full localization of electrons at interstitial atoms manifests itself in an isometrization due to ionic bonding. The Y-I distance, 3.095 Å, is in good agreement with the value 3.10 Å expected for pure ionic bonding.

Electrical properties

Measurements of the temperature dependence of electrical resistivity ρ on YIH_n ($n \leq 1$) revealed an interesting influence of the hydrogen content *n* on transport properties (Fig. 6). All samples show metallic behavior at high temperatures. However, they undergo a smooth metal-insulator transition with decreasing temperature as indicated by an increasing resistivity at low temperatures. The reduction of the H-content to its lower limit n = 0.61(3) is accompanied by a considerable increase of the resistivity and a minimum at 110 K. This finding is in contrast to expectations based on free

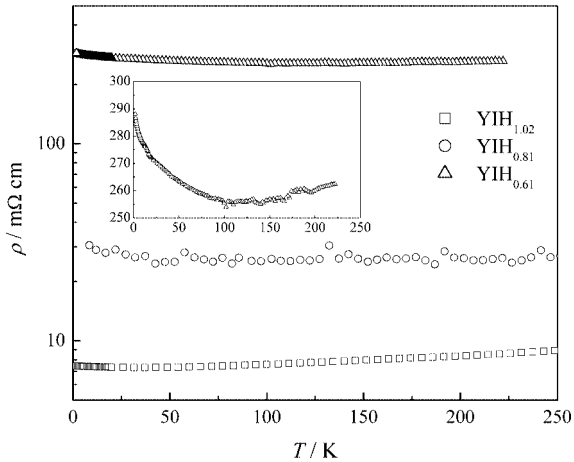

Fig. 6 Electrical resistivity ρ against T for YIH_n ($n \leq 1.0$). The inset picture shows the temperature dependence of ρ for $YIH_{0.61}$ on a large scale.

electrons, suggesting Anderson-type localization of electrons [33] in multi-center metal-metal bonding. The latter can originate from an ordering of the hydrogen atoms as *n* approaches the lower limit of the homogeneity range [10]. The electron localization in $YIH_{0.61}$ is further confirmed by magnetic measurements, which reveal a decrease of Pauli paramagnetism in comparison with that for $YIH_{0.81}$ [34].

Acknowledgement. We are grateful to *C. Kamella* for EDX analyses and *G. Siegle* for the resistivity measurements.

References

[1] G. Meyer, S.-J. Hwu, S. Wijeyesekera, J.D. Corbett, *Inorg. Chem.* **1986**, *25*, 4811.
[2] Hj. Mattausch, R. Eger, J.D. Corbett, A. Simon, *Z. Anorg. Allg. Chem.* **1992**, *616*, 157.
[3] F. Ueno, K. Ziebeck, Hj. Mattausch, A. Simon, *Rev. Chim. Miner.* **1984**, *21*, 804.
[4] Hj. Mattausch, W. Schramm, R. Eger, A. Simon, *Z. Anorg. Allg. Chem.* **1985**, *530*, 43.
[5] Hj. Mattausch, A. Simon, K. Ziebeck, *J. Less-Common Met.* **1985**, *113*, 149.
[6] C. Michaelis, *Diplomarbeit* , Univ. Stuttgart 1986.
[7] A. Simon, Hj. Mattausch, R. Eger, *Z. Anorg. Allg. Chem.* **1987**, *550*, 50.
[8] R. Müller-Käfer, *Dissertation*, Univ. Stuttgart 1988.
[9] Th. Schleid, G. Meyer, *Z. Anorg. Allg. Chem.* **1987**, *552*, 90.
[10] J. K. Cockcroft, W. Bauhofer, Hj. Mattausch, A. Simon, *J. Less-Common Met.* **1989**, *152*, 227.
[11] A. S. Izmailovich, S. I. Troyanov, V. I. Tsirelnikov, *Russ. J. Inorg. Chem.* **1974**, *19*, 1597.
[12] D. G. Adolphson, J. D. Corbett, *Inorg. Chem.* **1976**, *15*, 1820.
[13] R. L. Daake, J. D. Corbett, *Inorg. Chem.* **1977**, *16*, 2029
[14] O. Beckmann, H. Boller, H. Nowotny, *Monatsh. Chem.* **1970**, *101*, 945.
[15] G. Brauer, *Handbuch der Präparativen Anorganischen Chemie*, 3rd. ed., Vol. 2, F. Enke, Stuttgart 1978, pp. 1077.
[16] H. E. Flotow, D. W. Osborne, K. Otto, *J. Chem. Phys.* **1962**, *36*, 866.

[17] A. Sieverts, *Z. Metallk.* **1929**, *21*, 37.
[18] C. Michaelis, Hj. Mattausch, A. Simon, *Z. Anorg. Allg. Chem.* **1992**, *610*, 23.
[19] J. Körbl, *Mikrochim. Acta* **1956**, *11*, 1705.
[20] R. Eger, Hj. Mattausch, A. Simon, *Z. Naturforsch.* **1993**, *48b*, 48.
[21] J. Rodriguez-Carvajal, FullProf 2000, Program for the structure refinement with Rietveld analysis, LLB CEA-CNRS 2001.
[22] A. Simon, *J. Appl. Crystallogr.* **1971**, *4*, 138.
[23] H. Imoto, J. D. Corbett, *Inorg. Chem.* **1981**, *20*, 630.
[24] M. Ryazanov, A. Simon, Hj. Mattausch, *Z. Anorg. Allg. Chem.* **2004**, *630*, 104.
[25] K. R. Poeppelmeier, J. D. Corbett, *Inorg. Chem.* **1977**, *16*, 294.
[26] H. Krebs, *Grundzüge der Anorganischen Kristallchemie*, F. Enke, Stuttgart 1968, p. 224.
[27] R. Hoppe, *Adv. Fluorine Chem.* **1970**, *6*, 386.
[28] A. Simon, Hj. Mattausch, G. J. Miller, W. Bauhofer, R. K. Kremer, in: *Handbook on the Physics and Chemistry of Rare Earths*, Vol. 15, K. A. Gschneidner Jr., L. Eyring (eds), Elsevier Publ., Amsterdam-London-New York-Tokyo 1991, p. 191.
[29] H. M. Rietveld, *J. Appl. Crystallogr.* **1969**, *2*, 65.
[30] H. S. Marek, J. D. Corbett, R. L. Daake, *J. Less-Common Met.* **1983**, *89*, 243.
[31] U. Schwanitz-Schüller, A. Simon, *Z. Naturforsch.* **1985**, *40b*, 710.
[32] S.-J. Hwu, R. P. Ziebarth, J. V. Winbush, J. E. Ford, J. D. Corbett, *Inorg. Chem.* **1986**, *25*, 283.
[33] M. Cutler, N. F. Mott, *Phys. Rev.* **1969**, *181*, 1336.
[34] M. Ryazanov, A. Simon, R. K. Kremer, Hj. Mattausch, *to be published*.

